Electronic Couplings and Energy Transfer Dynamics in the Oxidized Primary Electron Donor of the Bacterial Reaction Center

Xanthipe J. Jordanides,*,†,§ Gregory D. Scholes,†,|| Warwick A. Shapley,‡ Jeffrey R. Reimers,*,‡ and Graham R. Fleming†

Department of Chemistry, University of California, Berkeley, and Physical Biosciences Division, Lawrence Berkeley National Laboratory, Berkeley, California 94720, and School of Chemistry, The University of Sydney, NSW 2006, Australia

Received: August 23, 2003; In Final Form: November 6, 2003

It has been known for 30 years that the oxidized special pair radical cation P^+ is as efficient as the neutral ground-state species P in quenching excitation from the neighboring accessory bacteriochlorophylls B_L and B_M, but the mechanism for this process has remained elusive. Indeed, simple treatments based on application of standard Förster theory to the most likely acceptor candidate fails by 5 orders of magnitude in the prediction of the energy transfer rates to P^+. We present a qualitative description of the electronic energy transfer (EET) dynamics that involves mixing of the strongly allowed transitions in P^+ with a manifold of exotic lower-energy transitions to facilitate EET on the observed time scale of 150 fs. This description is obtained using a three-step procedure. First, multireference configuration-interaction (MRCI) calculations are performed using the semiempirical INDO/S Hamiltonian to depict the excited states of P^+. However, these calculations are qualitatively indicative but of insufficient quantitative accuracy to allow for a fully a priori simulation of the EET and so, second, the INDO results are used to establish a variety of scenarios, empirical parameters that are then fitted to describe a range of observed absorption and circular dichroism data. Third, EET according to these scenarios is predicted using a generalized Förster theory that uses donor and acceptor transition densities, which together account for the large size of the chromophores in relation to the interchromophore spacings. The spectroscopic transitions of P^+ that facilitate the fast EET are thus unambiguously identified.

I. Introduction

The photosynthetic reaction center (RC) of purple bacteria is a pigment−protein complex present in the thylakoid membrane that, under low light intensity, efficiently accepts excitation energy either directly or from antenna complexes to initiate light-induced charge separation from the primary electron donor, a bacteriochlorophyll dimer (P); this is the first step in photosynthesis.[1] The photoexcited dimer (P*) then transfers an electron to either bacteriopheophytin acceptors H_L or H_M within three picoseconds[2] and with a quantum yield of nearly one.[3] If, however, the RC is exposed to high light conditions or a chemical oxidant, the primary electron donor[4] P^+ is directly formed and electron transfer and, in turn, photosynthesis are blocked. The radical pair P^+H^- is then generated and decays in about 200 ps. Under high light intensity conditions, P* can quench excitation by rapid electronic energy transfer (EET) from higher energy RC pigments, either from the monomeric "accessory" bacteriochlorophyll-*a* molecules (B_L and B_M) or from the bacteriopheophytins (H_L and H_M).[5−18] Four of the RC pigments are pictured in Figure 1. The absorption bleach of the accessory bacteriochlorophylls B, created by 800-nm light, recovers in ∼130 fs in the neutral RC due to fast EET. Throughout this manuscript, the term "neutral" is used to refer to the "unoxidized" reaction center. Remarkably, recovery also occurs in ∼150 fs in the oxidized RC.[9] In both cases, the ground-state recovery of the bacteriochlorophylls has been interpreted as arising following energy transfer to the special pair within the RC. It is hence clear that EET to the oxidized primary electron donor (from the accessory bacteriochlorophyll or from the antenna) still occurs,[5,8,9,19] despite the quite different natures of the acceptor states P and P^+.

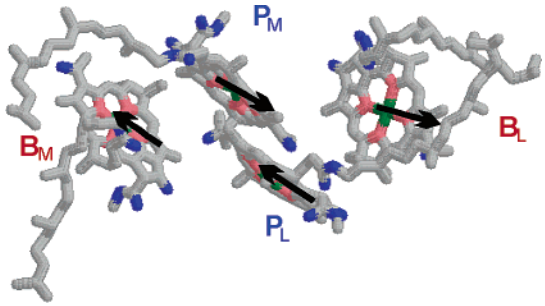

Figure 1. A view from the lumenal side of the membrane of the special pair of BChls; P_M and P_L and the accessory BChls, B_L, and B_M are shown. The arrows represent the *approximate* Q_y transition dipole moments for the localized excited states, which are very different than the Q_y directions taken from the QM/MM optimized structure.[20]

Why the neutral RC and oxidized RC primary electron employed donors are equally efficient quenchers of the excitation has been an unanswered question for the past 30 years and has led to speculation that a unique EET mechanism is at work in the RC. The main goal of this paper is to understand the experimental observation that P^+ readily quenches the excitation

* Corresponding authors. E-mail: xjj2@cornell.edu; reimers@chem.usyd.edu.au
† University of California and LBNL.
‡ The University of Sydney.
§ Present address: School of Applied and Engineering Physics, Cornell University, Ithaca, New York 14853.
|| Present address: Lash Miller Chemical Laboratories, 80 St. George Street, University of Toronto, Toronto, Canada M5S 3H6.

10.1021/jp036516x CCC: $27.50
Published on Web 01/10/2004

energy from B. The dominant changes in the absorption spectrum that occur upon oxidation are the appearance of two new bands, one at ~1250 nm (~8000 cm^{-1}) and another at ~4000 nm (~2600 cm^{-1}). Considering the acceptor state with the largest spectral overlap to the 800 nm B fluorescence (the ~1250 nm band of P^+) and assuming a dipole−dipole coupling mechanism, an EET time of ~10 ns is calculated, 5 orders of magnitude slower than the observed value. The failure of such standard energy transfer calculations, which are based on the spectral overlap between the donor emission and the acceptor absorption spectrum, motivated us to develop a new methodology for calculating energy transfer.[21,22] It has been postulated that energy transfer from B to P^+ could be mediated by short-range electronic interactions (e.g., electron exchange according to Dexter).[8,9,19] We show here that it is not necessary to include such corrections to the coupling. By elucidating the excited states of P^+ via quantum chemical calculations, then using these results as the basis for both modeling the absorption spectrum and calculating electronic couplings, using the transition density cube (TDC) method, we have developed an understanding of the mechanism of EET in the oxidized RC.

The marked dissimilarities between the electronic structures of the neutral dimer P and the radical dimer cation P^+ are revealed in their difference (oxidized minus neutral) spectra.[4,5,23−27] Due to the presence of strong coupling within the neutral molecular dimer P_LP_M, the excited state is split into states that are approximately symmetric (+) and antisymmetric (−) linear combinations of $P_L{}^*P_M$ and $P_LP_M{}^*$, denoted as the exciton states P_+ and P_- (not to be confused with P^+) for the special pair. The most dramatic change in the spectrum of the oxidized RC is the loss of the upper exciton P_- transition at 865 nm, which implies that the excitonic coupling within the dimer is disrupted. In addition, two new electronic transitions develop in the infrared: both a near-infrared transition at ~1250 nm (8000 cm^{-1})[4,13,23,28] and a mid-infrared transition at ~4000 nm (2600−2750 cm^{-1})[13,29,30] have been observed. However, neither of these transitions appears to provide sufficient spectral overlap to act as a viable energy acceptor in the EET pathway from B or H to P^+.

Previously, we have shown that in order to predict quantitatively the rates of EET to a neutral dimeric (or multimeric) acceptor, it is necessary to employ a generalized prescription of Förster theory.[21,22,31,32] We have recently developed and employed this generalized version of Förster theory to show that EET dynamics in the neutral RC are promoted via Coulombic couplings between the donor and acceptor pigments and that it is crucial to accommodate the multichromophoric nature of the donor and acceptor in the EET rate expression. We concluded that the upper exciton transition of the special pair P_+ is the principal acceptor state involved in energy transfer from B to P in the neutral RC and quantitatively predict the EET rate and its unexpected temperature independence without parameter adjustment.[22] Now, we turn to this generalized version of Förster theory to elucidate the energy transfer dynamics within the RC in the more complex case in which the special pair acceptor is a radical cation. We show that the key to understanding the mechanism of EET from the accessory B to the primary electron donor is to accurately describe the electronic and vibronic structures of the radical cation dimeric acceptor.

To model the EET in the RC, the following elements must to be considered: the arrangement of the pigments, the spectroscopy of the acceptor, the electronic couplings between pigments, the electron−phonon coupling, the vibrational frequencies, and the possibility of energetic disorder, i.e., differences in the site energies. The most significant feature differentiating the oxidized RC from the neutral reaction center, and any previously reported energy transfer systems of which we are aware, is that the acceptor is a dimeric radical. Therefore, we focus on determining the electronic energies and origins of the electronic transitions of the oxidized special pair acceptor and quantifying the electronic coupling between each of these relevant transitions and the donor transitions (B* → B, etc.).

Reimers and Hush have previously reported extensive quantum chemical calculations, using the semiempirical intermediate neglect of differential overlap (INDO/S) technique for the oxidized RC in the gas phase. In that work, a singles-excitation multireference configuration-interaction (MRCI−S) calculation was used to provide energies and assignments of the electronic transitions of the oxidized primary electron donor.[33−36] It is well accepted that the lowest energy state, near 2500 cm^{-1}, is dominated by the intervalence charge-transfer band $P_L{}^+P_M \rightarrow P_LP_M{}^+$,[29,33,34,37,38] though detailed simulation of this band[39] and examination of the spectrum for a variety of species[35,40] suggest that a SHOMO → HOMO transition is also involved. Most interest[33,39,41] has however, focused on analysis of the degree of charge delocalization over P_L and P_M. The next higher energy band, at ~8000 cm^{-1}, most likely originates from tripdoublet excitations.[33,35] Three higher energy transitions calculated by INDO/S lie between 10 000 cm^{-1} and 14 000 cm^{-1},[33] but have yet to be correlated with particular features in the experimental absorption spectrum. Despite experimental and theoretical studies of the radical cation P^+, fundamental questions remain about its electronic structure.

The present work reports the results of further INDO/S quantum chemical calculations that provide the acceptor transitions in the presence of the protein, where all chromophores (e.g., B, H, carotenoid, etc.) and the imidazole side chains of the coordinating histidines are treated quantum mechanically in a static dielectric protein medium. Although the spin pairing in the electronic states is complicated, we recognize that the overall spin in the dimer is conserved. Hence, electronic couplings to the allowed singlet transition of the donor states are Coulombic (or promoted by the dipole−dipole mechanism). Since the RC is a molecular aggregate and the distance between chromophores is smaller than the chromophore size, the transition density formalism is employed to calculate the Coulombic couplings between transitions.[42]

INDO/S is a semiempirical technique that provides qualitatively realistic descriptions of chromophores such as those considered herein, but it is not capable of delivering the quantitative accuracy required for a complete a priori simulation of the EET dynamics. In particular, significant errors in calculated transition energies can occur, transition moment magnitudes will be only approximate, and the dispersion-based intermolecular coupling that drives charge delocalization within P^+ is not present.[36] Further, vibronic couplings significantly redistribute[39] intensity within P^+, and these are not easily determined using electronic structure techniques.[43]

Time-dependent density-functional theory provides, in principle, a more accurate method for calculation of the electronic structure and is now becoming feasible for molecules of the size of a bacteriochlorophyll dimer. In preliminary calculations, we determined the excited states of P^+ by this technique using the B3LYP[44] density functional via the Gaussian 98 package,[45] obtaining a dense manifold of excited states of energy <14000 cm^{-1}. However, none of these states contained charge-transfer character but rather corresponded to localized transitions on each

bacteriochlorophyll. The significance of many of the calculated states is difficult to ascertain as modern density-functional theory dramatically underestimates the transition energies in extended conjugated systems.[46] While in general, modern density-functional theory is also poorly appropriate for charge-transfer processes,[47] its failure to describe the critically important charge-transfer states of P^+ arises from what in Hartree−Fock terms is interpreted as the single-reference-determinant nature of time-dependent density-functional theory. As the nature of the nonparticipatory electrons on each bacteriochlorophyll changes significantly upon electron transfer, excited states need to be described in terms of orbitals or densities that do not bias the calculations toward one particular localized-electron scenario. This requirement is met using our MRCI approach based on INDO/S but is not included within the framework of time-dependent density-functional theory. Hence, the only electronic structure method currently available for systems of this size that can provide a qualitatively realistic description of the excited states of P^+ is INDO.

The ability of P^+ to quench the excitation energy in photosynthesis is a well-known, yet incompletely understood, phenomenon. Explaining the mechanistic details of this experimental observation is the main motivation of this paper, and the theoretical approach is summarized below. Details of the INDO computational method, the means used to determine electronic couplings, and the transition density method[42] of generalized Förster theory used to describe interactions between molecules whose size is of the order of the intermolecular spacings are given in section II. Their application to model the EET dynamics is provided in section IV, but first in section III a series of scenarios is developed through which the qualitatively descriptive INDO results can be adapted to provide quantitative descriptions of the absorption and circular dichroism spectra of the system. In the conclusions (section V) it is shown that only one of the feasible scenarios leads to a robust description of the observed fast EET process, thus identifying an important mechanism that operates to quench unwanted absorbed energy during photosynthesis under high-light conditions.

II. Methods

A. Computational Quantum Chemistry. For all calculations, a semiempirical INDO method, as previously described,[33] is employed. MRCI−S is performed with either single (−S) or single plus some double excitations (−S+D); two equally weighted reference determinants that represent the ground states of P^+ with the electron hole localized either on P_L or P_M are implemented. Calculations performed in this manner provide comparable descriptions of both internal transitions within each bacteriochlorophyll and charge-transfer transitions between the two. When included, the double excitations for the monomer bacteriochlorophylls, also applied to both reference determinants, are from the highest occupied molecular orbital (HOMO) and the second-highest occupied molecular orbital (SHOMO) to the lowest unoccupied molecular orbital (LUMO) and the second lowest unoccupied molecular orbital (SLUMO). Before the CI calculation, the molecular orbitals are either localized on one-half of the special pair dimer (localized) or retained in their original canonical form (canonical).

To obtain realistic in situ geometries for these calculations, a combined QM (quantum mechanics)/MM (molecular mechanics) method is employed where all cofactors BChl, BPhe, carotenoid, and the imidazole side chains of the histidines are treated quantum mechanically. The remaining protein residues are treated via molecular mechanics simulation, which was used to adjust the coordinates of the pigments.[20,48] A protein dielectric constant of 2.0 was employed to implicitly include polarizability effects.[20,48] Thus, all semiempirical calculations are performed on this QM/MM optimized geometry of the reaction center according to the method described in detail in references 20 and 48. Additionally, density functional calculations (B3LYP) were also performed as a self-consistency check of the results.

The transition densities, TD, were also obtained using these methods for individual molecules. The Coulombic electronic couplings, V^{Coul}, are calculated from the INDO transition density, TD. The INDO TD is a density matrix in the atomic center (monopole and dipole) representation where the number of points in the transition density is the number of atomic centers (e.g., for $BChl_a$ this corresponds to 98 atomic centers). The INDO transition density accounts for the exact shape and size of the molecule, but takes on a form simpler than that which appears in ab initio transition density cube methods[42] in that the transition density is localized purely at atomic centers and can be represented in terms of just atomic charges and atomic dipoles. This is a necessary consequence of the INDO Hamiltonian, which neglects differential overlap. Strictly speaking, only the atomic charge contribution should actually appear because only this term can be expressed in terms of INDO energy, but the atomic dipole contribution is usually added as an empirical correction known as the "hybridization contribution" because this is necessary in order to obtain semiquantitative descriptions of molecular transition moments.[49]

B. Electronic Couplings. To calculate the EET rate using the adapted Förster theory for molecular aggregates we need as input electronic couplings between the basis states that will be mixed to generate the effective donor and acceptor states, and, in turn, the effective electronic couplings. We have calculated these couplings using transition densities for donor and acceptor transitions that were calculated using semiempirical quantum chemical methods.

The transition density P_A between electronic states g and e of molecule A relates to $|\Psi_e\rangle\langle\Psi_g|$ and is defined as[50,51]

$$P_A(ge|\boldsymbol{r}_1) = N\int \Psi_e(\boldsymbol{x}_1,\boldsymbol{x}_2,...\boldsymbol{x}_N)\Psi_g^*(\boldsymbol{x}'_1,\boldsymbol{x}'_2,...\boldsymbol{x}'_N)\, d\boldsymbol{x}_2...d\boldsymbol{x}_N\, d\boldsymbol{x}'_2...d\boldsymbol{x}'_N d\boldsymbol{s}_1 d\boldsymbol{s}'_1 \quad (1)$$

where $\boldsymbol{x}$ is a function of the spin variable $\boldsymbol{s}$ and the position variable $\boldsymbol{r}$. N is the number of electrons in molecule A and the spin variable $\boldsymbol{s}_1$ has been integrated out. For the transition density we note that $\int P_A(ge|\boldsymbol{r}_1)\, d\boldsymbol{r}_1 = 0$. The transition dipole moment $\boldsymbol{M}_A^{eg}$ is calculated by applying the dipole operator to the transition density according to

$$\boldsymbol{M}_A^{eg} = \int \boldsymbol{r}_1 P_A(ge|\boldsymbol{r}_1)\, d\boldsymbol{r}_1 \quad (2)$$

The INDO TD is a reduction of the full transition density of A and is represented as distributed monopoles and dipoles located at each atomic center i,

$$P_A(ge|\boldsymbol{r}_1) = P_A{}^i(ge|\boldsymbol{r}_1) \quad (3)$$

Each contribution to the TD is written using the standard multipole expansion[52] according to

$$P_A{}^i(ge|r_1) \approx q_A^{i,ge}\delta(\boldsymbol{r}^i - \boldsymbol{r}_1) + \boldsymbol{\mu}_A^{i,ge}\cdot\nabla\delta(\boldsymbol{r}^i - \boldsymbol{r}_1) \quad (4)$$

Equation 4 localizes transition density to the atomic centers where $q_A^{i,ge}$ is the transition atomic charge and $\boldsymbol{\mu}_A^{i,ge}$ is the

transition atomic dipole; higher-order terms (quadrupole, multicenter, etc.) do not appear, as described earlier. Similarly to eq 2, we sum over atomic centers to obtain

$$\boldsymbol{M}_{\mathrm{A}}^{eg} = \sum_i [\boldsymbol{r}^i q_{\mathrm{A}}^i + \boldsymbol{\mu}_{\mathrm{A}}^i] \tag{5}$$

which is written in a reduced notation where electron label 1 and the electronic transition label *ge* are dropped. To calculate the Coulombic coupling between INDO TDs of eq 3, the interaction potential between molecule A and molecule D is expanded in terms of a power series in R^{-1}, where $R \equiv R_{ij} = |\boldsymbol{r}_i - \boldsymbol{r}_j|$ is the distance between the i atomic center of molecule A and the j atomic center in molecule D, according to

$$V^{\mathrm{Coul}} = \frac{1}{4\pi\epsilon_{\mathrm{o}}} \sum_{i,j} \{q_{\mathrm{A}}^i q_{\mathrm{D}}^j + (\mu_{\mathrm{A},\alpha}^i q_{\mathrm{D}}^j - q_{\mathrm{A}}^i \mu_{\mathrm{D},\beta}^j)\nabla_\alpha - \mu_{\mathrm{A},\alpha}^i \mu_{\mathrm{D},\beta}^j \nabla_\alpha \nabla_\beta\} R_{ij}^{-1} \tag{6}$$

where the variables α and β are used to denote the components of the acceptor and donor transition dipole moments vectors, respectively. Using the identities $\nabla_\alpha R^{-1} = -\hat{R}_\alpha R^{-2}$ and $\nabla_\alpha \nabla_\beta R^{-1} = (3\hat{R}_\alpha \hat{R}_\beta - \delta_{\alpha\beta})R^{-3}$,[53] eq 6 becomes

$$V^{\mathrm{Coul}} = \frac{1}{4\pi\epsilon_{\mathrm{o}}} \sum_{i,j} \left\{ \frac{q_{\mathrm{A}}^i q_{\mathrm{D}}^j}{R_{ij}} + \frac{\hat{R}_\alpha}{R_{ij}^2}(q_{\mathrm{A}}^i \mu_{\mathrm{D},\beta}^j - \mu_{\mathrm{A},\alpha}^i q_{\mathrm{D}}^j) - \frac{(3\hat{R}_\alpha \hat{R}_\beta - \delta_{\alpha\beta})}{R_{ij}^3} \mu_{\mathrm{A},\alpha}^i \mu_{\mathrm{D},\beta}^j \right\} \tag{7}$$

Similar expressions have been derived by a number of authors.[53−56] By making the substitutions $\delta_{\alpha\beta} \rightarrow \alpha\cdot\beta$ and $\hat{R}_\alpha \rightarrow \alpha\cdot\hat{R}$[57]

$$V^{\mathrm{Coul}} \cong \frac{1}{4\pi\epsilon_{\mathrm{o}}} \sum_{i,j} \left(\frac{q_{\mathrm{A}}^i q_{\mathrm{D}}^j}{R_{ij}} + \frac{q_{\mathrm{A}}^i (\boldsymbol{\mu}_{\mathrm{D}}^j \cdot \hat{\boldsymbol{R}}_{ij})}{R_{ij}^2} - \frac{(\boldsymbol{\mu}_{\mathrm{A}}^i \cdot \hat{\boldsymbol{R}}_{ij}) q_{\mathrm{D}}^j}{R_{ij}^2} - \frac{3(\boldsymbol{\mu}_{\mathrm{D}}^j \cdot \hat{\boldsymbol{R}}_{ij})(\boldsymbol{\mu}_{\mathrm{A}}^i \cdot \hat{\boldsymbol{R}}_{ij}) - \boldsymbol{\mu}_{\mathrm{A}}^i \cdot \boldsymbol{\mu}_{\mathrm{D}}^j}{R_{ij}^3} \right) \tag{8}$$

is obtained and used throughout this work to determine the Coulombic couplings that mediate electronic energy transfer. The dipole−dipole coupling V^{dd}, along with the orientation factor, may then be calculated

$$V^{\mathrm{dd}} = \frac{|\sum_i \boldsymbol{r}^i q_{\mathrm{A}}^i + \boldsymbol{\mu}_{\mathrm{A}}^i| \cdot |\sum_j \boldsymbol{r}^j q_{\mathrm{D}}^j + \boldsymbol{\mu}_{\mathrm{D}}^j| \kappa}{4\pi\epsilon_{\mathrm{o}} R^3} \tag{9}$$

where $\kappa \equiv \hat{\boldsymbol{r}}_{\mathrm{A}} \cdot \hat{\boldsymbol{r}}_{\mathrm{D}} - 3(\hat{\boldsymbol{r}}_{\mathrm{A}} \cdot \hat{\boldsymbol{R}})(\hat{\boldsymbol{r}}_{\mathrm{D}} \cdot \hat{\boldsymbol{R}})$. At sufficiently large donor−acceptor separations, the shape of the transition densities is insignificant in determining the electronic coupling and $V^{\mathrm{Coul}} \sim V^{\mathrm{dd}}$.

C. Energy Transfer Dynamics for Molecular Aggregates. The key components that are incorporated into the theory for EET in molecular aggregates are (1) explicit separation of electronic and nuclear factors in the rate expression, (2) calculation of the effective electronic couplings using the basis set of the molecules that comprise the aggregate, (3) careful calculation of the nuclear spectral overlap factors, (4) association of each electronic coupling between donor (δ) and acceptor (α) $V_{\delta\alpha}$ with a corresponding spectral overlap factor $J_{\delta\alpha}(\epsilon)$, where ϵ is the energy scale, to generate the dimensionless coupling-weighted spectral overlap for each interaction, $u_{\delta\alpha}(\epsilon) = |V_{\delta\alpha}|^2 J_{\delta\alpha}(\epsilon)$, and (5) taking an ensemble average over many aggregates. Under the assumptions that (1) coupling is weak between donors and acceptors (but not *among* either donors or acceptors) and (2) energy transfer is incoherent and occurs from the fully relaxed donor, an expression for the rate of energy transfer from donor states δ to acceptor states α that incorporates all these concepts is given by[21]

$$k = \frac{2\pi}{\hbar} \langle \int_0^\infty \mathrm{d}\epsilon \sum_{\delta,\alpha} P_\delta |V_{\delta\alpha}(\epsilon_{\mathrm{d}},\epsilon_{\mathrm{a}})|^2 J_{\delta\alpha}(\epsilon,\epsilon_{\mathrm{d}},\epsilon_{\mathrm{a}}) \rangle_{\epsilon_{\mathrm{d}},\epsilon_{\mathrm{a}}} \tag{10}$$

where $V_{\delta\alpha}$ are the electronic couplings between the effective donors and acceptors, and ϵ_{d} and ϵ_{a} represent static offsets from the mean of the donor and acceptor excitation energies to characterize the difference in the pigment site energies as a result of the different protein environments, as previously described.[21] Thus it is emphasized that both the couplings and the spectral overlaps depend on disorder. It is assumed that each $V_{\delta\alpha}(\epsilon_{\mathrm{d}},\epsilon_{\mathrm{a}})$ does not vary across the energy spectrum of its corresponding $J_{\delta\alpha}(\epsilon,\epsilon_{\mathrm{d}},\epsilon_{\mathrm{a}})$. P_δ is a normalized Boltzmann weighting factor for the contribution of δ to the thermalized donor state, $P_\delta = \exp[(\epsilon_{\delta=1} - \epsilon_\delta)/kT] / \sum_\delta \exp[(\epsilon_{\delta=1} - \epsilon_\delta)/kT]$. The angle brackets denote that an ensemble average is taken over many aggregate units (e.g., RC complexes) so as to account for static disorder in the monomer site energies. The spectral overlap between bands δ and α is defined in terms of donor and acceptor densities of states,[21]

$$J_{\delta\alpha}(\epsilon,\epsilon_{\mathrm{d}},\epsilon_{\mathrm{a}}) = N_\alpha a_\alpha^{\mathrm{hom}}(\epsilon,\epsilon_{\mathrm{d}},\epsilon_{\mathrm{a}}) N_\delta f_\delta^{\mathrm{hom}}(\epsilon,\epsilon_{\mathrm{d}},\epsilon_{\mathrm{a}}) \tag{11}$$

Note that each $J_{\delta\alpha}(\epsilon,\epsilon_{\mathrm{d}},\epsilon_{\mathrm{a}})$ is associated with an electronic coupling factor $V_{\delta\alpha}(\epsilon_{\mathrm{d}},\epsilon_{\mathrm{a}})$ within the ensemble average. The $f_\delta^{\mathrm{hom}}(\epsilon,\epsilon_{\mathrm{d}},\epsilon_{\mathrm{a}})$ and $a_\alpha^{\mathrm{hom}}(\epsilon,\epsilon_{\mathrm{d}},\epsilon_{\mathrm{a}})$ specify the donor and acceptor densities of states, respectively. The acceptor density of states is written as

$$a_\alpha^{\mathrm{hom}}(\epsilon,\epsilon_{\mathrm{d}},\epsilon_{\mathrm{a}}) = \sum_l P(l) \mathrm{Re} \int_0^\infty \mathrm{d}t \langle l|l(t)\rangle \exp[i(\epsilon - \epsilon_\alpha^l)t/\hbar] \times \exp[-g(t)] \tag{12}$$

where l denotes the vibrational modes, and $\langle l|l(t)\rangle$ represents the time-dependent overlap of the initial ground-state vibration l with its evolution in the excited electronic state, which is a time-domain representation of the Franck−Condon factors. The superscript "hom" specifies the line shape in the absence of disorder (i.e., homogeneous line broadening only). The homogeneous line shape function is defined in the usual manner using $g(t)$ as described in detail elsewhere.[22] The corresponding absorption line shape for the acceptor A is defined by

$$a_{\mathrm{A}}(\epsilon) = \langle \sum_\alpha |\mu_\alpha|^2 a_\alpha^{\mathrm{hom}}(\epsilon) \rangle \epsilon \tag{13}$$

Correspondingly, the fluorescence line shape for the donor D is defined by

$$f_{\mathrm{D}}(\epsilon) = \langle \sum_\delta |\mu_\delta|^2 f_\delta^{\mathrm{hom}}(\epsilon) \rangle \epsilon^3 \tag{14}$$

where μ_α is the transition moment of state α and the angular brackets denote an ensemble average over the static disorder in the site energies. The emission density of states (DOS) is given by

TABLE 1: Summary of the Calculated (INDO/MRCI−S) Properties (transition dipole moments, μ and transition energies, ΔE of transitions) for Oxidized *Rb. sphaeroides* RC[a]

state	type	probability[b]	$\|\mu\|$ (Debye)	f [c]	$\hat{\mu}$ (x,y,z)	ΔE, cm^{-1}
B_L	^1Q_y	0.92	8.55	0.46	(0.79, 0.45, 0.43)	13400
B_M	^1Q_y	0.92	8.87	0.49	(−0.96, 0.01, 0.30)	13100
H_L	^1Q_y	0.92	6.79	0.39	(0.19, −0.97, −0.16)	17900
H_M	^1Q_y	0.92	6.71	0.38	(0.28, −0.32, −0.90)	18200
P_1^+	hole transfer	0.97	3.29	0.021	(−0.44, −0.61, 0.66)	4220
P_2^+	^3Q_y(M)	0.81	0.27	0.00030	(0.69, 0.63, −0.36)	8950
P_3^+	SH → H(L^+)	0.66	0.38	0.00074	(−0.60, −0.79, −0.13)	10700
P_4^+	HT + ^3Q_y(L)	0.70	1.09	0.0070	(0.96, 0.19, −0.22)	12600
P_5^+	^1Q_y(M)	0.69	8.16	0.46	(−0.84, −0.53, −0.10)	14800
P_6^+	HT + SH → H(M^+)	0.58	0.78	0.0056	(1.00, 0.0031, −0.043)	15838

[a] These are the INDO/MRCI−S assignments of P_3^+ and P_4^+ are not authoritative assignments. In fact, a recent density functional calculation assigns the shoulder of 2200 cm^{-1} to the SH→ H(L^+) transition.[40] [b] The assignments of the P^+ eigenstates are made according to the one-electron transitions (determinants) with the largest probability (CI state coefficient). [c] The oscillator strength of each transition.

$$f_\delta^{\text{hom}}(\epsilon) = \sum_k P(k)\text{Re}\int_0^\infty dt\langle k|k(t)\rangle \exp[i(\epsilon - \bar{\epsilon}_\delta^k + 2\lambda)t/\hbar] \times \exp[-g^*(t)] \quad (15)$$

Here it is assumed that vibrational relaxation and thermalization have occurred prior to emission (and therefore prior to energy transfer). λ is the reorganization energy associated with the Stokes shift and $\langle k|k(t)\rangle$ is the time-dependent overlap of the initial excited-state vibration k with its evolution in the excited electronic state. A detailed description of the theory and the implementation can be found in references 21 and 22, respectively.

We can think of the donor states δ as collectively comprising the donor emission spectrum and the acceptor states α as collectively comprising the acceptor absorption spectrum. For each δ and α we wish to calculate $|V_{\delta\alpha}(\epsilon_d,\epsilon_a)|^2 J_{\delta\alpha}(\epsilon,\epsilon_d,\epsilon_a)$—the dimensionless quantity that defines the rate of $\delta\rightarrow\alpha$ EET. For this strategy to work, the $V_{\delta\alpha}$ must be classified as "weak." To determine $J_{\delta\alpha}(\epsilon,\epsilon_d,\epsilon_a)$ we need electron−phonon coupling information together with intramolecular vibrational information in terms of a line shape function or spectral density. We can input this information using explicit equations, but since the line shape information is contained in experimental emission and absorption spectra (in the absence of significant inhomogeneous line broadening), experimental spectra may also be used, as our group has shown, for the calculation of EET from the carotenoid to bacteriochlorophyll in LH2.[31]

III. The Nature of P^+: Electronic States and Absorption Spectrum

A. Transition Energies and Dipole Strengths. The calculated transition dipole moments and energies for all the pigments in the oxidized RC are shown in Table 1. Since INDO is parametrized to obtain the energies and dipole strengths of the $\pi \rightarrow \pi^*$ transitions that are in good agreement with the experimental absorption spectrum, scaling of the TD by some factor such as $\mu_{\text{exp}}/\mu_{\text{calc}}$[42] in order to obtain the true electronic couplings, as is often required in ab initio applications, is naively not expected to be as crucial here. However, the μ_{calc} reported here, when compared to μ_{exp} for $BChl_a$[58] and BPh_a[58] in acetone, are approximately 1.3 and 1.1 times larger, respectively. Nevertheless, the calculated transition energies for the neutral pigments do accurately predict the experimentally determined energy ordering of the BChl and BPhe pigments[18,59−62] of E(H_M) > E(H_L) > E(B_L) > E(B_M), suggesting that the major influence of the protein environment on the transition energies is through geometrical distortions of the chromophores. Thus, the QM/MM method employed here[20] provides a means to investigate subtle structural effects associated with protein asymmetry, as previously shown by Reimers and co-workers who predicted the structural changes in 22 reaction center mutants from *Rb. sphaeroides*.[48]

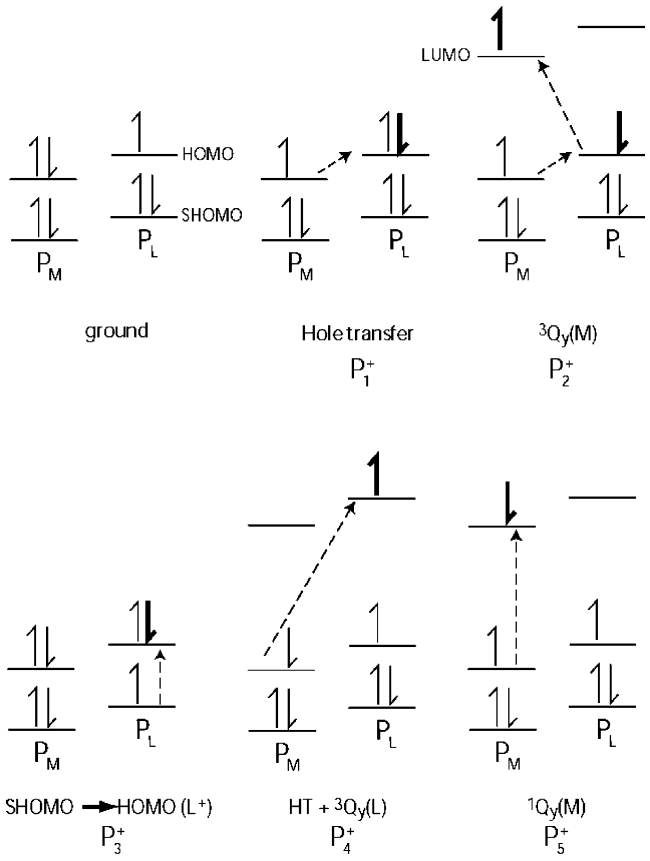

Figure 2. Some doublet electronic states (within the 4-orbital model) of the special pair cation. The second-highest occupied molecular orbital (SHOMO), the highest occupied molecular orbital (HOMO), and the lowest unoccupied molecular orbital (LUMO) are all shown. For each dimer half, one-electron determinants are expressed in terms of localized HOMO and LUMO orbitals for the oxidized special pair, P^+. For the *Rb. sphaeroides* RC we calculate E(P_L) > E(P_M), which results in localization of the hole on P_L. Electrons that participate in a given transition are drawn in bold.

The nature of the special pair dimer cation transitions, also provided in Table 1, will now be discussed. The P_1^+ to P_6^+ eigenstates (or CI states) are obtained after diagonalizing the

Hamiltonian in the basis of spin-adapted excited-state determinants. These determinants are obtained as single excitations from a set of reference determinants obtained using the Gouterman four-orbital (per macrocyle) model[63] to assign the seven highest-energy electrons of P^+ to the four highest-energy occupied orbitals in all possible ways. The assignments of the P^+ eigenstates are made according to the one-electron transitions (determinants) with the largest probability (CI state coefficient). As shown in Table 1, the extent of the mixing between states of different "type" in some transitions is much larger than in others. The most important determinants for the special pair cations are shown in Figure 2; for simplicity, they are expressed in terms of a notation depicting states with charges localized on one-half of the special pair, which is typical of the nature of states predicted by INDO/S. Analogous descriptions in terms of charge-delocalized states may easily be generated, however, and in many cases may be more appropriate. For example, if the symmetry of the dimer radical cation is broken substantially, then the localized description $P_L^+P_M$ or $P_LP_M^+$ is most appropriate. However, if the C_2 symmetry largely persists, P^+ will be delocalized over the dimer and the representations ^2B or ^2A are more appropriate. In principle, the INDO/S calculations are free to mix the localized states shown in Figure 2 in determining the nature of the excited states of the system to any degree. However, as this method does not include the substantial dispersive component of the interaction energy, the actual degree of delocalization is expected to be underestimated.

Much experimental and theoretical effort has been devoted toward determining the asymmetry of the *Rb. sphaeroides* reaction center. Electron−nuclear double resonance spectroscopy determines the symmetry in the ground state and finds that the hole is not equally shared by the two BChls of the special pair dimer P^+, but is localized rather on the P_L side of the dimer as indicated by the spin densities of P_L to P_M, which are 5:1 at 20 K[64] and 2:1 at 298 K.[65] Modeling of the line shape of the hole-transfer absorption band confirms this analysis.[39] Using Stark spectroscopy to probe the degree of delocalization of an electronic transition, Boxer and co-workers find a small amount of asymmetry with more electron density on the P_M side, which was attributed to the H-bond to the C═O on the M side of the dimer that increases the electron density.[66,67] Also, the ground-state $P_L^+P_M$ has the hole localized on the L side of the special pair cation dimer. Although the placement of additional electron density on the P_M qualitatively agrees with some experiments, the delocalized representation seems more appropriate for some transitions. For example, Boxer and co-workers determined that the 1250 nm transition of P^+ is largely delocalized over the two bacteriochlorophylls of the special pair due to the very small change in dipole moment.[28] They also recently determined that significant delocalization must be employed to model the Stark spectrum of the ∼4000 nm transition.[30]

The results in Table 1 include only singly excited states. Additionally including doubly excited states (+D) yields similar assignments and energy ordering of all transitions except for ^1Q_y(M), which has the same oscillator strength, but is predicted by MRCI−S+D to have a wavelength of 755 nm, compared to 675 nm for CIS. Including double excitations to all other electronic states (non-^1Q_y(M) transitions) overcorrelates the ground state, which lowers the ground-state energy and, as a result, overestimates the transition energy. Localized MRCI−S+D calculations were also performed and yielded similar results, giving us confidence in the results reported herein.

The spin-allowed, (doublet) one-electron transitions (shown in Figure 2 and Table 1) have been described extensively elsewhere,[68] thus will only briefly be explained here. The transition P_1^+ corresponds to the lowest energy transition at ∼2600 cm^{-1} (∼4000 nm) first observed by Breton and co-workers.[29] It has been attributed to the intervalence hole transfer band.[29,33,34,37,38,41] Although this transition is too low in energy to accept excitation energy from the antenna or from B/H in the oxidized reaction center, it is included for completeness in the calculation of the absorption spectrum. The next higher energy transition P_2^+, with a calculated energy of 8950 cm^{-1}, was discovered many years ago in the oxidized reaction center P^+ at ∼8000 cm^{-1} (∼1250 nm).[4,13,23,28] Reimers and Hush suggested that this band originates from a triplet-coupled (tripdoublet) transition.[33] As shown in Figure 2, this transition arises from two spin-allowed excitations from the ground state, but is denoted ^3Q_y(M) because at large P_L-P_M separation it correlates to the forbidden Q_y triplet absorption (HOMO → LUMO transition) on P_M. The P_3^+ transition corresponds to local excitation of the charged P_L by promoting an electron from its SHOMO to HOMO. SHOMO to HOMO transitions on a charged monomer have been proposed previously for the oxidized special pair.[29,37,38] SCF-based methods such as INDO/S are expected to significantly overestimate the energy of transitions of this type, and it is likely that this transition is actually observed as a shoulder at 2200 cm^{-1} on the low-frequency side of the hole-transfer band.[40] In the one-electron picture, the P_4^+ transition corresponds to a single excitation from the HOMO of P_M to the LUMO on P_L. Similar to the ^3Q_y(M) transition, at large intradimer separation, the energy of the ^3Q_y(L) +HT transition corresponds to the sum of a HT transition and triplet absorption of P_L. The last calculated transition depicted in Figure 2 is P_5^+, which represents the singlet-coupled ^1Q_y(M) because at large separation it corresponds to the spin-allowed HOMO to LUMO excitation on the neutral M side of the dimer.

As a check on the INDO results for P^+, a time-dependent density functional theory calculation (gas phase using B3LYP/3-21G) was also carried out. The calculated SHOMO → HOMO energy changed to 3200 cm^{-1}, but third-HOMO and fourth-HOMO to HOMO transitions were also predicted at 4080 and 4470 cm^{-1}, respectively. The three triplet-coupled absorptions, predicted to occur at 9090, 9240, and 9850 cm^{-1}, correspond to mixed excitations of predominantly ^3Q_x(M), what seems to be ^3B_y(L), and ^3Q_y(M), respectively. The three singlet coupled excitations occurring at 10 300, 13 500, and 13 700 cm^{-1} correspond predominantly to ^1Q_y(M), ^1Q_y(L), and ^1Q_x(M), respectively. As mentioned previously, time-dependent density-functional theory underestimates significantly transition energies in extended conjugate systems and severely overestimates the energies of the most important hole-transfer excitations, none of which appears in the above list. For chromophore-localized excitations that are well represented using this approach, we see qualitative patterns similar to that predicted by INDO, though significant differences in the calculated transition energies occur.

B. Calculated Electronic Couplings. We have employed the INDO/MRCI−S TD on the QM/MM optimized RC complex to determine the Coulombic couplings between the various pigments in the oxidized RC from *Rb. sphaeroides.* The Coulombic couplings between the Q_y of BChl, Q_y of BPhe donors, and the first five acceptor P^+ transitions are shown in Table 2. As previously noted, the dipole strength obtained using our INDO/MRCI−S method is slightly larger than the experimentally determined dipole strengths for BChl and BPhe. Thus, the electronic couplings calculated between those pigments may be overestimated by a factor of ∼1.4. Experimental dipole

TABLE 2: Electronic Couplings (cm^{-1}) in the Oxidized RC from *Rb. sphaeroides* (including the P^+ transitions and the Q_y transitions of B and H)[a]

	V_{mn}^{Coul} (V_{mn}^{Coul}, scaled)/$V_{mn}^{Coul+vibronic}$											
transition	B_L			B_M			H_L			H_M		
B_L, ^1Q_y				45			202			−17		
B_M, ^1Q_y							−14			184		
H_L, ^1Q_y										9		
P_1^+, HT	55	(110)/	−74	−94	(−188)/	−103	−2	(−4)/	21	−2	(−4)/	−13
P_2^+, ^3Q_y(M)	1	(12)/	124	5	(60)/	14	1	(12)/	−21	0.3	(4)/	11
P_3^+, SH → H(L^+)	3	(30)/	−108	27	(270)/	19	0.1	(1)/	20	−0.5	(−5)/	−10
P_4^+, HT + ^3Q_y(L)	9	(45)/	153	−33	(−165)/	−23	−3	(−15)/	−29	−6	(−30)/	7
P_5^+, ^1Q_y(M)	−263	(−263)/	−286	−19	(−19)/	0	47	(47)/	47	−23	(−23)/	−25

[a] V_{mn}^{Coul} is calculated from eq 8 using the INDO transition density. V_{mn}^{Coul}, scaled is Coulombic coupling with the scaled acceptor transition dipole moment for P_n^+ where $n \neq 5$ according to Table 3. $V_{mn}^{Coul+vibronic}$ is the Coulombic and vibronic contribution to the coupling, which is calculated according to eqs 18, 19, and 20 using the vibronic mixing coefficients given in Table 3.

strengths of the P^+ transitions have not been reported; therefore, a comparison to our calculated values cannot be made.

As expected, the couplings between the BChl and BPhe are the largest for nearest neighbor pigments, e.g., B_L-H_L and B_M-H_M, which have center-to-center separations of 11.2 and 11.9 Å, respectively. The asymmetry of the electronic couplings to the radical cation transitions partly corresponds to the asymmetry of the calculated electronic couplings (using the INDO/MRCI−S TD) in the neutral RC: $V(B_L-P_M) = -216\ cm^{-1}$ versus $V(B_L-P_L) = 4\ cm^{-1}$. These large differences arise from the mutual orientation of the transition dipole moments of the BChl pigments as shown in Figure 1. Thus, if a radical cation transition is predominantly localized on P_M, as is the case for ^1Q_y(M), it has a correspondingly larger coupling to B_L than to B_M. Similarly, if the radical cation transition predominantly involves the ^1Q_y transition of P_L, e.g., P_3^+ or SH→ H(L^+), the electronic coupling to the ^1Q_y transition of B_M is larger than to the ^1Q_y transition of B_L. The electronic couplings to $P_5{}^+$ or ^1Q_y(M) transition reveal the most dramatic effect of this asymmetry. In the oxidized special pair, the hole is localized on P_L, which places more electron density on P_M and results in a larger asymmetry than in the neutral RC.

To investigate the effect of specific protein residues on the electronic couplings, calculations were performed without the imidazole residues coordinating B_M, B_L, P_M, and P_L. The electronic couplings between the neutral pigments, $V(B_L-H_M)$, etc., are largely unaffected (less than 2%), whereas the electronic couplings to the cation P^+ transitions, $V(H/B-P^+)$, either decrease or increase by as much as 50%. Electronic couplings in the neutral RC (from *Rb. sphaeroides* and *Rps. viridis*) obtained using the MRCI−S/INDO TD (including the effects of Mg ligands and the effects of CIS vs CIS+D) and the point dipole approximation have also been calculated.[69] As shown in Table 2, the numerical calculations of the electronic couplings differ significantly depending on the model employed, but as will be shown in section IV, the final qualitative conclusion regarding the EET mechanism remains unaltered.

C. The P^+ Absorption and Circular Dichroism Spectra. *(i) Calculation Strategy.* To understand the absorption spectrum and, in turn, the energy transfer dynamics within the oxidized reaction center, a calculation of bare electronic eigenstates (exciton "sticks") is insufficient. Donor and acceptor line shape functions are necessary to reproduce the absorption spectrum and to calculate the donor and acceptor spectral overlaps. Also recall that coupling of an electronic transition to intramolecular vibrations and to nuclear fluctuations of the solvent not only broaden the width of the absorption band but also lead to a shift in the transition frequency. Additional frequency shifts of the absorption bands of a molecular aggregate, such as the RC, arise from electronic interactions between localized electronic states. Experimental feedback, provided by absorption, emission, and circular dichroism spectra, is useful when employing the INDO/CI−S method to calculate electronic transition energies since it generally cannot predict the absolute pigment energies to the accuracy required.

We employ a strategy whereby the calculated site energies, and in some cases dipole strengths, are systematically varied in order to simulate both the experimental absorption and circular dichroism spectra. The Hamiltonian in the site representation, containing the adjusted site energies for each localized electronic state as well as the electronic couplings between these states, is diagonalized to mix the states. The eigenstates are dressed according to an appropriate line shape function (cf. eq 12). We note that such a procedure is most useful when the states are relatively weakly mixed. A Monte Carlo ensemble-averaging procedure was performed over 1000 to 2000 RC pigment complexes to account for static disorder in the site energies. The reason we use a "simulate-and-compare" procedure, rather than deconvolving the absorption spectrum using a line shape decomposition method, is that we need to be able to model the spectral overlaps between every pair of effective donor and acceptor states $J_{\delta\alpha}$. When applying the conventional Förster theory to understand the absorption spectrum of a molecular aggregate, spectral overlap information is entangled with the electronic couplings, thus making its application effectively useless. In our adapted Förster theory, we calculate donor δ and acceptor α states and their associated $J_{\delta\alpha}$ and $V_{\delta\alpha}$ values in order to compute the overall energy transfer rate according to eq 10.

(ii) Features of the Experimental Absorption Spectrum. The experimental visible electronic absorption spectra (650−1200 nm or ∼8000−15000 cm^{-1})[70] for the RC from *Rb. sphaeroides* before (neutral RCs (dashed line)) and after titration by the oxidizing agent potassium ferricyanide (solid lines) are shown in Figure 3a.[70] Upon oxidation, a 5 nm blue-shift in the B band and a 2 nm red-shift of the H band have been observed.[4,5,23,25−27,71] These band shifts are largely electrochromic in origin; that is, the field created by the formation of the charged special pair dimer induces shifts of the B and H bands.[62] Owing to these B and H band frequency shifts, the P^+ minus P difference electronic spectrum is difficult to interpret in the visible region due to the resultant large first-derivative-like components. Hence, the P^+ transitions in this 12000 to 14000 cm^{-1} spectral region are almost completely obscured by the B and H bands,

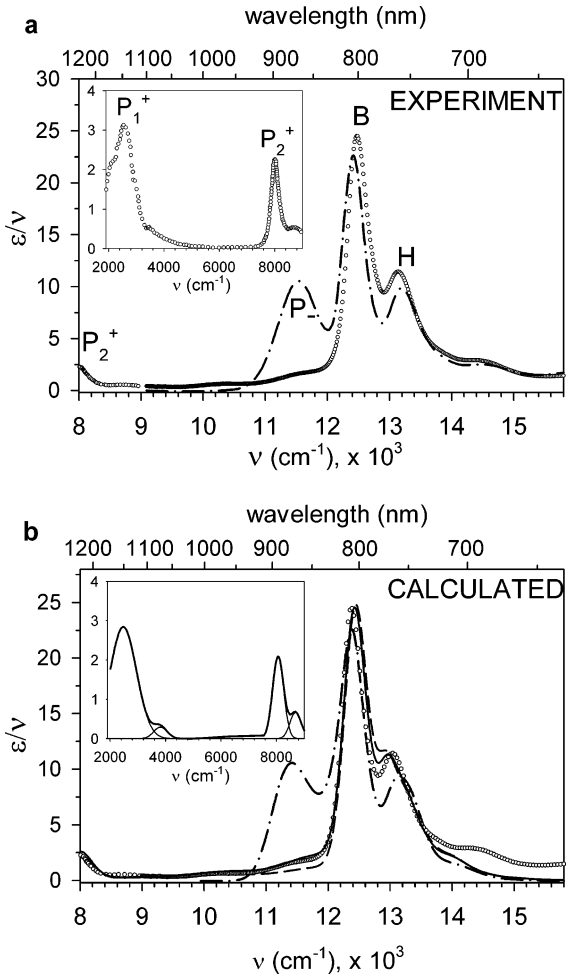

Figure 3. (a) Experimental[70] and (b) calculated absorption spectra of the neutral (dashed-dotted line) and the oxidized RC (circles, dashed, and solid lines) from *Rb. sphaeroides*. (a, inset) Experimental[72] and (b, inset) calculated mid-infrared light-dark difference spectra in the near-IR range. (b) To calculate the absorption spectra, a dipole moment scaling (dashed line) and a vibronic scaling (solid line) are employed and compare well to the experiment oxidized spectrum (circles). The calculated neutral spectrum is also shown (dashed-dotted line). Notes: The inset of (b) employs Gaussian fits to the P_1^+ and P_2^+ bands. The neutral spectrum does not exhibit features at P_1^+ and P_2^+.

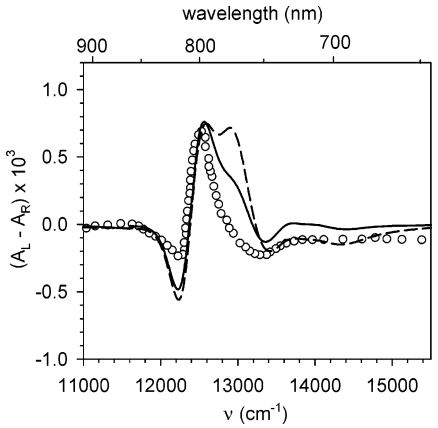

Figure 4. Experimental[23] (circles) and calculated (lines) circular dichroism spectra of the oxidized RC from *Rb. sphaeroides*. Two calculation methods are compared: the "dipole moment scaling" (dashed line) and the "vibronic coupling" (solid line).

even in the P^+ minus P difference spectrum, and as a result it is nearly impossible to uniquely assign all the potential energy acceptor states of P^+.

Other significant spectral changes in the visible region of the spectrum are also evident and aid in assigning the band positions and shapes of the oxidized special pair acceptor transitions. Namely, the lower exciton transition P_- at 865 nm and the upper exciton transition P_+ at 815 nm both disappear. Breton and coworkers have provided experimental evidence via linear dichroism to support the complete loss of these transitions.[73] It is important to note that simulations of the neutral RC absorption spectrum that neglect the P_- and P_+ transitions produce the following intensity depletions: a 5% loss of H band and a 10% loss of the B band. In addition, upon oxidation a sizable increase in the absorption under and between the B and H bands is evident. This finding is not unique to the experimental spectra presented here; a consistent increase in absorption intensity of the B and H bands corresponding to ~10% increase in the absorption in this region was observed as early as 1970,[4,5,23−27] but remains unexplained. An increased absorption at near-infrared wavelengths greater than 930 nm (10750 cm^{-1}) in the oxidized spectrum is revealed by the nonzero baseline in Figure 3a. A simple baseline correction of the near-infrared portion of the visible spectrum would give the false impression that any potential states lower in energy than the B band have exactly zero oscillator strength.

The experimental infrared difference spectrum (1100−4500 nm or ~2000−9000 cm^{-1})[72] for the oxidized special pair is shown in the inset of Figure 3a. The ratio of the infrared spectrum to the visible spectrum was fixed to the intensity ratio of the B band to the P^+ band at 1250 nm (~8000 cm^{-1}), which was determined to be ~17:1 from an oxidized spectrum from 200 to 1400 nm.[23] Two new infrared transitions at ~1250 nm (8000 cm^{-1}) and ~4000 nm (2600−2750 cm^{-1}) are clearly evident in the IR difference spectrum (see Figure 3a). These bands are the most clearly resolved P^+ transitions and have therefore been the most thoroughly studied. A recent quantitative simulation[39] of the band shape of just the 4000 nm band required the inclusion of up to 10^9 vibronic states. This state cannot act as a possible energy acceptor for excitation transfer from the accessory bacteriochlorophylls; however, and herein we focus only on the P_n^+ transitions that can. While the vibronic descriptions that we provide for all electronic states are clearly simplistic, nonetheless we expect our model to elucidate a correct and lucid physical model of the EET dynamics that is appropriate for our present study.

(iii) Calculated P^+ Absorption and Circular Dichroism Spectra. The parameters employed to calculate the absorption and circular dichroism spectra in the visible and near-infrared regions are provided in Table 3. Column one gives the transition type that is determined using the INDO/MRCI−S calculation as explained in section A. The increased reorganization energy in the line shape functions of the special pair cation, when compared to the 100 cm^{-1} reorganization energy λ of the upper and lower exciton states of the neutral RC, necessitates an additional broadening mechanism. This increased λ may originate from the varying degree of localization of a given transition and could also explain the nonuniform reorganization for each P_n^+ transition. For example, we have simulated the neutral RC absorption spectrum with a λ for the localized B and H transitions that is two times smaller than the λ of the delocalized P_+ and P_- transitions. The coupling to intramolecular modes is another broadening mechanism that can be employed to understand the very broad absorption line shapes of the oxidized special pair. To this end, we explicitly include resonance Raman frequencies and displacements[74,75] in the line broadening function of the ~1250 nm transition. The energetic disorder of the

TABLE 3: Summary of the Parameters Employed to Calculate the Absorption Spectrum: Reorganization Energy, λ, of the Electron−Phonon Coupling, Energetic Disorder, Energy Shift, Dipole Scaling Factor, and Vibronic Mixing Coefficient, λ_n^v, for the Oxidized *Rb. sphaeroides* Reaction Center

transition	λ^a cm^{-1}	Γ_{inhom} cm^{-1}	energy shift cm^{-1}	dipole moment scaling	λ_n^v
B_L	280	55[b]	−900	1	1
B_M	280	55[b]	−700	1	1
H_L	280	55[c]	−5000	1	1
H_M	280	55[c]	−5000	1	1
P_1^+	400	55[c]	−1400	*2	0.49
P_2^+	280	55[c]	−1000	*12	−0.47
P_3^+	1000	55[c]	−1300	*10	0.42
P_4^+	800	55[c]	−1400	*5	−0.55
P_5^+	800	55[c]	−1800	1	N/A

[a] Total reorganization energy used to fit the absorption band. The reorganization energy arising from intramolecular vibrational modes is 200 cm^{-1} (for B, H, P_2^+ only) and is determined using $\lambda = \hbar \sum_i S_i \omega_i$. The reorganization energy due to electron−phonon coupling that arises primarily from intermolecular modes is determined using $M(t) = \lambda \exp(-t^2/\tau^2)$ where τ (fs) is taken from photon echo measurements of the RC B band.[76] [b] From Raman excitation profiles in reference 74. [c] Assumed to be the same as the accessory BChls.

P^+ transitions is assumed to be identical to that in the neutral RC.[22] To match the energy of the P_n^+, BChl, and BPh transitions to the observed values, a red-shift of the calculated MRCI−S energies (in Table 1) is necessary. The experimental spectrum in Figure 3a aids in positioning the energies of the calculated electronic states P_1^+−P_5^+ formed upon oxidation of the special pair and the resulting energy shifts are given in Table 3.

In simulating the absorption spectrum of the oxidized RC, the dipole strengths of the P_1^+−P_4^+ transitions are appreciably underestimated by the INDO/MRCI−S calculations. To explain the enhancement of the absorption strength, three different models based on a vibronic coupling formalism have been examined. Within this formalism, interaction occurs between the nuclear and electronic motions of a molecule, and the transition moments are written as a sum of a purely electronic (Coulombic) component and a vibronically induced component:

$$\vec{\mu}_n^{\text{exp.observed}} = \vec{\mu}_n^{\text{Coul+vib}} = (\vec{\mu}_n^{\text{Coul}} + \vec{\mu}_n^{\text{vib}}) \approx (\vec{\mu}_n^{\text{calculated}} + \lambda_n^v \vec{\mu}_{P_5^+}^{\text{Coul}}) \quad (16)$$

In eq 16, n is any acceptor transition P_n^+ (other than P_5^+) that mixes with P_5^+ according to the vibronic mixing coefficient, λ_n^v, giving rise to borrowed excitation intensity from the strongly allowed P_5^+ transition. It is important to recall that "Coul" refers to the Coulombic coupling calculated using the INDO transition densities according to eq 8. Since the sum of ϵ/ν must be conserved, the P_5^+ transition will lose intensity as determined by

$$\vec{\mu}_{P_5^+}^{\text{Coul+vib}} \approx (\vec{\mu}_{P_5^+}^{\text{Coul}} - \sum_{n \neq P_5^+} \lambda_n^v \vec{\mu}_n^{\text{Coul}}) \quad (17)$$

Since dipole strength $|\vec{\mu}_n^{\text{exp·observed}}|^2$ is the experimental observable, determining λ_n^v in eq 16 requires solving a quadratic equation and results in two roots. Each root provides in principle a unique scenario through which the results of the INDO calculations can be related to the experimentally observed spectra. Taking the smallest root is equivalent to assuming that the INDO-calculated allowed intensity forms the bulk of the observed extinction, with the vibronic contribution being of minor importance, while taking the largest root assumes that the vibronic coupling is extremely large and its effects are in fact negated by the allowed electronic coupling. Calculations of the CD spectrum performed using these two assumptions reveal that only use of the smaller root leads to sensible predictions, and, for the sake of brevity, we proceed considering only this root. However, to further explore this issue, later we consider the scenario, more likely than the interference-based hypothesis presented by use of the upper root, that *only* vibronic coupling is of importance. Meanwhile, for the smallest root, using the dipole strengths reported in Table 1 and eq 16 above, the mixing coefficients for a given acceptor transition n, λ_n^v, are calculated and vary from −0.55 to 0.49 as shown in the last column of Table 3. Employing a vibronic coupling mechanism to explain the forbidden intensity, according to eqs 16 and 17, changes not only the magnitude of the transition dipole moment but also its direction. These new vector directions will, in turn, affect the CD spectrum because it critically depends on an accurate determination of the pigment orientation.

An important implication of the vibronic coupling to the transitions of P^+ is that the electronic couplings also need to be corrected for the vibronic coupling contributions.[77] EET can be mediated by vibronically induced transitions. In that case one can think of the Coulombic coupling between transition densities, where one or both may be of a higher excited state of the molecule, but mixed with the relevant donor or acceptor transition through vibronic coupling. This is accounted for explicitly using the calculated vibronic mixing coefficients λ_n^v and approximated by writing the electronic coupling between the donor state m and the P^+ acceptor state n according to

$$V_{mn}^{\text{Coul+vibronic}} \approx V_{mn}^{\text{Coul}} + V_{mn}^{\text{vib}} \quad (18)$$

$$V_{m-n\neq P_5^+}^{\text{Coul+vibronic}} \approx (V_{m-n\neq P_5^+}^{\text{Coul}} + \lambda_n^v V_{m-n=P_5^+}^{\text{Coul}}) \quad (19)$$

$$V_{m-n=P_5^+}^{\text{Coul+vib}} \approx (V_{m-n=P_5^+}^{\text{Coul}} - \sum_{n\neq P_5^+} \lambda_n^v V_{m-n}^{\text{Coul}}) \quad (20)$$

where eqs 19 and 20 are for the non-P_5^+ and P_5^+ acceptor states, respectively. The resulting electronic couplings will not only perturb the steady-state spectra such as absorption and CD, but they will also alter the energy transfer dynamics, as will be shown in the next section.

Now that the effects of vibronic coupling on the transition moment and electronic couplings are understood, we present and employ three model scenarios for relating the INDO-derived spectral properties to the observed absorption and circular dichroism spectra: (1) a linear scaling of the P_1^+−P_4^+ transition dipole moments according to the "dipole moment scaling" factor given in Table 3; (2) a "vibronic coupling" scaling of all P_1^+−P_5^+ transitions based on a vibronic coupling scheme of eqs 16 and 17 above, where, for example, the weakly allowed P_1^+ transition gains absorption strength by vibronically coupling to the strongly allowed P_5^+ transition; and (3) a model in which the allowed transition moments are completely ignored, where $\vec{\mu}_n^{\text{Coul}}$ and V_{mn}^{Coul} are both zero, and which will be referred to as the "vibronic only" model.

By employing the "dipole moment scaling" method, scaling factors as large as 10 (see Table 3) are obtained and the corresponding scaled electronic couplings, "V_{mn}^{Coul}, scaled," are

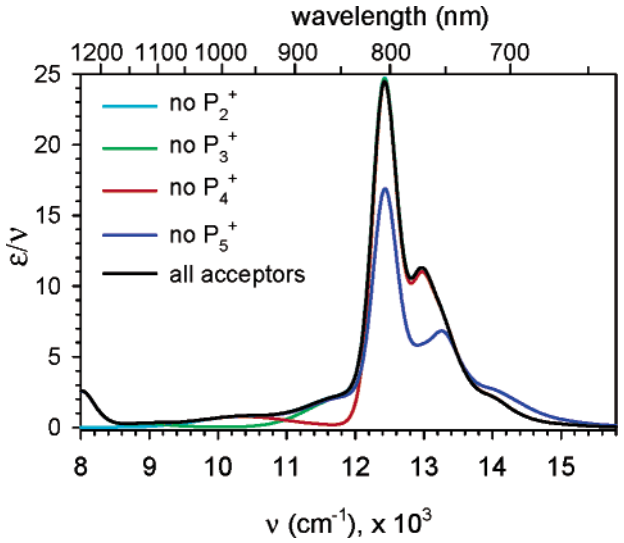

Figure 5. Calculated absorption spectra, excluding some of the relevant P^+ acceptor states.

provided in parentheses in Table 2. The scaling of method (1) is analogous to renormalization of the Franck−Condon allowed intensity for the first four P^+ transitions. Using these scaled dipole moments and couplings, the absorption and CD spectra are calculated and, as shown in Figures 3b and 4, respectively, reproduce the general features moderately well. The necessity of such large scaling factors suggests that these acceptor P^+ transitions contain significant borrowed intensity, probably as a result of vibronic coupling to the strongly allowed P_5^+ transition.[78] Thus, rather than simply scaling the transition moments, which would increase the transition dipole moment of the non-P_5^+ transitions, and correspondingly linearly increase in the coupling to each transition, our second approach, model (2), is to explain the additional intensity using a "vibronic coupling" scheme. Using the previously calculated vibronic mixing coefficients λ_n^{ν} and eqs 16−19, the "vibronic coupling" transition dipole moments and couplings are calculated (Table 2) as are the absorption and CD spectra (Figures 3b and 4, respectively). This "vibronic coupling" model improves the simulation of the absorption spectra and CD when compared to the "dipole moment scaling" method. A change in the CD spectrum is expected because the vibronically induced scaling model not only affects the intensity of each the transition but also affects the transition dipole moment orientations. However, the differences in the calculated absorption and CD spectra when employing models (1) and (2) are small when compared to the large range of the calculated couplings (see Table 2). Thus, although the couplings vary between the two models, the spectra are not drastically affected.

To demonstrate the spectral positions and the role of intensity borrowing between the radical cation transitions P_3^+−P_5^+, we calculate an absorption spectrum with $\vec{\mu}_n^{\text{Coul+vib}} = 0$ for each n (Figure 5). Within the "vibronic coupling" calculation of the absorption spectrum, the following statements can be made: the increase in intensity in the near-IR region (between 900 and 1200 nm) is mainly due to P_3^+, the shoulder on the red-edge of the B band is primarily P_4^+, and the P_5^+ transition plays a significant role in mixing with B and H transitions and correspondingly donates intensity to those bands in the spectrum. Thus, the change in intensity of the absorption and CD spectra after the RC is oxidized can only be explained using a scheme in which intensity is borrowed from P_5^+. Although the exact position of P_5^+ cannot be determined here, the CD, which is remarkably sensitive to its site energy and absorption spectra, are useful aids in determining its energy.

TABLE 4: Energies and Composition of the Exciton Eignenstates in Terms of Percentage Monomer Contributions at 298 K for the Oxidized RC from *Rb. sphaeroides*[a]

exciton state	energy eigenvalue (cm^{-1})	P_1^+	P_2^+	P_3^+	P_4^+	P_5^+	B_L	B_M	H_L	H_M
1	2378	**100**	0	0	0	0	0	0	0	0
2	7941	0	**100**	0	0	0	0	0	0	0
3	9392	0	0	**100**	0	0	0	0	0	0
4	11190	0	0	0	**98**	0	2	0	0	0
5	12272	0	0	0	2	16	**52**	21	8	1
6	12375	0	0	0	0	6	15	**74**	2	3
7	12906	0	0	0	0	37	0	0	**63**	0
8	13035	0	0	0	0	**40**	31	0	27	2
9	13227	0	0	0	0	1	0	5	0	**94**

[a] The donor and acceptor exciton states are defined by the pigment with the largest composition and are used to calculate the energy transfer dynamics. Calculated using the "vibronic coupling" method, i.e., by employing the couplings $V_{mn}^{\text{Coul+vib}}$ in Table 2 according to eq 19.

Despite the comparative success of the previous two models, the "vibronic only" method (model 3 and results not shown) fails to reproduce the absorption and CD spectra as well as the previous two models. The "vibronic only" model produces (a) identical transition dipole directions for all P_n^+ transitions (according to eq 16), and (b) nearly zero vibronic coupling between the P_5^+ transition and all other B/H transitions, which according to eq 19 yields $V_{m-P_5^+}^{\text{Coul+vib}} \approx 0$ for all transitions except for $V_{B_L-P_5^+}^{\text{Coul+vib}} \approx -20\ \text{cm}^{-1}$. As shown by the exciton state composition of the "vibronic coupling" model (Table 4), mixing between the P_5^+ and the B_L, B_M, and H_L transitions (in exciton states 5, 6, 7, and 8) is strong. Calculating the electronic couplings using generalized Förster theory allows the superexchange-type pathways that result from the strong mixing to be appropriately included. Moreover, the nonzero electronic coupling to the strongly allowed P_5^+ transition, $V_{m-P_5^+}^{\text{Coul}}$, which provides the exciton delocalization, is critical in explaining the absorption increase observed in the B/H region of the spectrum and in reproducing the general trend of the CD spectrum. To the contrary, the "vibronic only" model produces a high degree of localization (99% of exciton state 7 is the P_5^+ transition); thus, although important, a vibronic coupling mechanism cannot be used *exclusively* to understand the oxidized special pair spectroscopy in the RC.

IV. Energy Transfer Mechanism from B To P^+

At this point we have established a reasonable understanding of the spectroscopy of the acceptor, P^+, which has enabled us to identify possible acceptor states and estimate line shapes that are required for spectral overlap calculations. We have furthermore determined realistic electronic couplings, based on calculated transition densities, between the donors and each P^+ acceptor transition. Moreover, it is now evident that it is important to consider vibronic coupling in order to account for the intensity of the P^+ transitions, which in turn will modify the magnitude and nature of the electronic couplings. Finally, we have seen that some of the P^+ states mix significantly with the donor states. We can account for the implications of this mixing, to a first approximation, by employing the generalized Förster theory model so that superexchange-type pathways for EET are taken into consideration. Bringing all these details together has enabled us to assemble a qualitative understanding of the mechanism of EET flow in the oxidized RC.

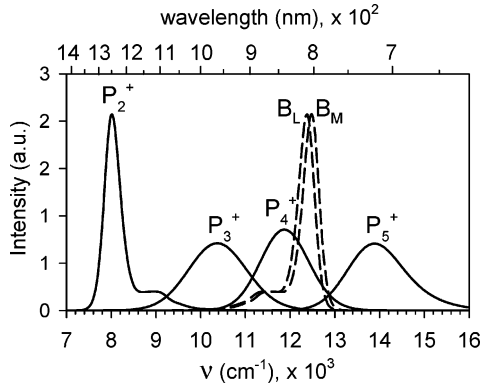

Figure 6. Calculated densities of states for the oxidized *Rb. sphaeroides* RC at 298 K. The density of states of the donor B_L/B_M (dashed lines) and the acceptor P_2^+ (~1250 nm) to P_5^+ (~740 nm) transitions were calculated using the "vibronic coupling" model as described in the text.

As shown in Figure 3, the most dominant changes in the absorption spectrum that occur upon oxidization are the appearance of two new features: the P_2^+ band at ~1250 nm (~8000 cm^{-1}) and the P_1^+ band at ~4000 nm (~2600 cm^{-1}). The spectral overlap between either of these P^+ absorption bands and the B emission band is clearly very small. Indeed, considering just these states and the calculated dipole−dipole electronic couplings, we determine an overall B-to-P^+ electronic energy transfer time of ~10 ns. The electronic couplings are not large enough to compensate for the insufficient spectral overlap between the B emission and the P_2^+ absorption spectra, and thus P_2^+ cannot act as a viable energy acceptor in the EET pathway from B to P^+. In pursuit of a more viable acceptor state, we consider the next three higher energy INDO/S calculated transitions P_3^+ to P_5^+ as potential acceptor states.

Using the parameters in Tables 2 and 3, the densities of states of these plausible acceptor states and the $B_{L/M}$ donor states are calculated and have the following maxima: P_3^+ at 970 nm, P_4^+ at 845 nm, P_5^+ at 740 nm, B_L at 809 nm, and B_M at 801 nm (Figure 6). The spectral overlaps, $J_{\delta\alpha}$, between the donor (δ) and the acceptor (α) states, where $\delta = B_M$ or B_L and $\alpha = P_n^+$, are determined using eq 10 and given in Table 5. From these spectral overlaps, and the electronic couplings, $V_{\delta\alpha}$, the energy transfer times $\tau_{\delta\alpha}$ between the donor BChl and the acceptor P^+ states are calculated. To determine the energy transfer rate, each $J_{\delta\alpha}$ is weighted by the square of the electronic coupling $|V_{\delta\alpha}|^2$ to give the corresponding coupling-weighted spectral overlap $|V_{\delta\alpha}|^2 J_{\delta\alpha}(\epsilon)$ for each pathway,[21,22,79] which after integration ($\int d\epsilon |V_{\delta\alpha}|^2 J_{\delta\alpha}(\epsilon)$) gives a value directly proportional to $1/\tau_{\delta\alpha}$, the energy transfer rate for each pathway.

These energy transfer time scales $\tau_{\delta\alpha}$ are shown in Table 5 for the oxidized RC. As discussed previously, the INDO/S calculations do not predict the correct charge delocalization in the special pair; therefore, conclusions regarding the rates along the different M and L branches cannot be made. Thus, it is useful to take a sum over the two donor B states (B_M and B_L) so as to model the average B to P^+ EET times; this is accomplished by performing $\sum_\delta P_\delta |V_{\delta\alpha}|^2 J_{\delta\alpha}(\epsilon)$ on eq 9, which results in the average EET times shown in the last column of Table 5. Although there are quantitative differences between the $\tau_{\delta\alpha}$ results of (1) the "dipole moment scaling" and (2) the "vibronic coupling" method, what is immediately obvious and, thus, the most significant feature of Table 5, is that any of the acceptor states have the ability to quench the excitation energy from the donor accessory BChl on the subpicosecond to picosecond time scale, in agreement with experiment.[9] In the previous section we showed that the "vibronic coupling" model slightly improves the simulation of the steady-state spectra, but it is important to point out that the qualitative scenario that arises is independent of the model employed since both models reproduce the main experimental features. However, the "vibronic coupling" method is strongly favored over the "dipole moment scaling" model because it is based on substantive physical insight and is thus, much less arbitrary. The scaling approach is also inferior because it relies on a correct assignment of the P^+ states because the dipole allowed intensity of each transition is scaled. Within the vibronic coupling mechanism, most of the intensity originates from vibronic coupling and the nature of the small allowed transition moments becomes irrelevant.

TABLE 5: Effective Electronic Couplings $V_{\delta\alpha}$ (cm^{-1}), Spectral Overlaps $J_{\delta\alpha}$(cm), and Energy Transfer Times $\tau_{\delta\alpha}$ (fs) between the Donor, δ, and Acceptor, α, States

pigments	$V_{\delta\alpha}$	$J_{\delta\alpha}$	$\tau_{\delta\alpha}$	$\tau_{B\alpha}$
(1) "Dipole moment scaling"method: calculated using "V_{mn}^{Coul} scaled" in Table 2				
$B_MP_3^+$	221	4.7×10^{-5}	370	270
$B_LP_3^+$	153	3.6×10^{-5}	990	
$B_MP_4^+$	157	4.7×10^{-4}	73	70
$B_{LP}P_4^+$	32	4.1×10^{-4}	2100	
$B_MP_5^+$	−161	2.7×10^{-5}	1200	210
$B_LP_5^+$	274	4.3×10^{-5}	260	
(2) "Vibronic coupling:" method: calculated using $V_{mn}^{Coul+vib}$ in Table 2				
$B_MP_3^+$	70	4.9×10^{-5}	3500	1500
$B_LP_3^+$	−85	4.0×10^{-5}	2900	
$B_MP_4^+$	−95	4.8×10^{-4}	200	80
$B_LP_4^+$	125	4.3×10^{-4}	130	
$B_MP_5^+$	−178	2.4×10^{-5}	1100	240
$B_LP_5^+$	283	3.5×10^{-5}	300	

[a] $\tau_{B\alpha}$ is the average energy transfer time considering that there are two possible donor states (B_M and B_L), i.e., $\sum P_\delta |V_{\delta\alpha}|^2 J_{\delta\alpha}(\epsilon)$ on eq 10.

The key to understanding the qualitative agreement between the calculated and experimental EET rates is in the calculated couplings: the INDO transition density calculation of the electronic couplings $V_{m-P_n^+}^{Coul}$ (given by eq 8) together with the vibronic coupling mechanism $V_{m-P_n^+}^{vib}$ (given by eqs 18, 19, and 20), which further enhances the couplings, provide a possible energy-transfer pathway for any of the three acceptor states (P_3^+, P_4^+, and P_5^+). The couplings in Table 5 differ from those in Table 2 because generalized Förster theory accounts for superexchange-type pathways (Table 4) involved in EET. These couplings may be the more correct representation of the physical picture because of the strong mixing between the radical cation transitions. Nonetheless, implementation of generalized Förster theory to calculate EET in the oxidized special pair is not necessarily required to retrieve the basic physics of the problem if transition densities for the P^+ dimer transitions are calculated. It is evident that only pairwise rates between B and P^+ transitions need to be calculated. However, because P^+ is a dimer, it is crucial to calculate electronic couplings between the B donor and P^+ acceptor states using their transition densities rather than a point dipole model. As we have shown previously, the point dipole approximation cannot account for the subtleties that arise owing to the arrangement of chromophores in a molecular aggregate, and thus does not capture, even qualitatively, the EET mechanism. Transition densities, on the other hand, contain all the necessary information on the spatial extent of the interchromophore coupling. Such information can also be accounted for by using a site representation for the chro-

mophores and the generalized Förster model, as we showed in our previous studies of the RC,[21,22] but this is more difficult for the case of the oxidized RC. In addition, we note that interactions that depend explicitly on orbital overlap between donor and acceptor have an insignificant influence on the EET dynamics in the RC aggregate and are ignored. But, orbital overlap within the P dimer, including nonorthogonality effects, are implicitly included in the calculation of the P^+ transition densities.

We now proceed to determine the most viable energy acceptor. P_5^+ is a likely energy acceptor and can act to quench the B excitation on a time scale that is in reasonable agreement with the recovery of the ground-state B absorption spectrum, ~150 fs,[9] but this transfer would have to occur uphill energetically. On this basis, we might rule out P_5^+ as the most viable acceptor state. However, P_5^+ plays an essential role via intensity mixing with the lower-lying states. It thus provides, indirectly, the means by which either P_3^+ or P_4^+ can accept energy on time scales that are in qualitative agreement with the experimental EET time (80−1500 fs). Calculations suggest that P_4^+ might be the more plausible energy acceptor as the rates are more comparable to those determined experimentally: average energy transfer times of ~70 fs and ~80 fs with the two methods.

The underlying mechanism of energy transfer in the oxidized RC is now addressed. The qualitative understanding of the EET mechanism is that the strongly allowed P_5^+ transition facilitates the more weakly dipole-allowed and transitions to become effective energy acceptors. The limitations of the INDO/S calculations described above prevent definitive assignments for some of the electronic transitions. Accordingly, we have focused on gaining qualitative insight by studying the feasibility and underlying mechanisms of the energy transfer. Fortunately, the assignment of the weakly dipole allowed states $P_1^+-P_4^+$ is relatively unimportant because most of their absorption intensity originates from the vibronic coupling mechanism and not from their calculated transition dipole moments (as given in Table 1). In addition, there is a manifold of vibronically enhanced, potential-acceptor transitions in the absorption spectrum, as shown in Figures 5 and 6. Of these potential acceptor states, P_3^+ ($f = 0.00074$) and P_4^+ ($f = 0.0070$) vibronically couple to P_5^+ ($f = 0.46$), giving rise to an enhanced excitation amplitude and providing adequate spectral overlap with B. A transition density cube calculation of the total electronic and vibronic coupling indicates that the P_3^+ and P_4^+ transitions sufficiently couple to B and become effective energy acceptors. Thus, the physical picture that emerges is a series of states all vibronically coupled to P_5^+ and having sufficiently large coupling and spectral overlap to quench the excitation energy from B on a time scale comparable to experiment.

V. Conclusions

Despite the very different energy-level structure of the oxidized and neutral special pairs, the energy transfer rate from B is surprisingly similar in both reaction centers. Thus, the main goal of this paper is to understand the experimental observation that P^+ quenches the excitation energy from B within ~200 fs. If the only energy quencher is assumed to be the ~1250 nm band observed in the absorption spectrum, the calculated Förster EET time is 10 ns: a time scale nearly 5 orders of magnitude slower than experiment. In this paper, we have resolved this conundrum by obtaining qualitative agreement (70−1500 fs depending on the acceptor state) with the experimental ultrafast EET time; the most likely acceptor state is identified to be P_4^+, which is observed at 12600 cm^{-1} and tentatively assigned to a hole-transfer plus tripdoublet excitation. Furthermore, an understanding of the steady-state spectra and the underlying mechanism of the time-dependent dynamics in the oxidized RC emerges.

Three main conclusions arise regarding the oxidized RC spectroscopy: (1) A detailed electronic structure calculation using INDO/MRCI−S of the excited states of the special pair cationic doublet states yields a manifold of weakly allowed states spanning the oxidized RC spectrum in addition to one strongly allowed acceptor state. (2) Employing the transition density formalism for the dimeric doublet transition densities is the key to calculating both the electronic couplings and EET rate. In this case, the INDO transition density is spread out across the two special pair molecules and accounts for the exact shape and size of the acceptor molecules, a feature completely lost when applying the dipole operator. (3) Our calculation shows that the strongly dipole-allowed transition (P_5^+) lends intensity to the other oxidized special pair states (P_3^+ or P_4^+). This explains the changes that occur in the absorption and CD spectra upon oxidation and provides the additional coupling for P_3^+ or P_4^+ to become viable quenchers of the excitation energy from B. This vibronic coupling mechanism, in which the weakly allowed acceptors vibronically borrow intensity from a strongly allowed acceptor and become candidates for EET transfer, is the fundamental mechanism that facilitates quenching of the excited-state accessory bacteriochlorophyll. A correct assignment of all the possible P^+ transitions is not a prerequisite for understanding the EET transfer dynamics since the vibronic coupling mechanism employed here relies only on the presence of some weakly allowed states anywhere across the spectrum, which can borrow intensity from the well-characterized $^1Q_y(M)$ P_5^+ transition. Although the precise acceptor state has not been uniquely determined here, further experiments will aid in resolving the energies of these oxidized special pair transitions.

Acknowledgment. We thank Professor Steve Boxer and Dr. Tom Treynor for their experimental P^+ data. The work carried out at UC Berkeley was supported by the Director, Office of Science, Office of Basic Energy Sciences, Chemical Sciences Division, U.S. Department of Energy under Contract DE-AC03-76SF000098. J.R.R. thanks the Australian Research Council and the Australian Partnership for Advanced Computing for funding this research. G.D.S. acknowledges the financial support of the Natural Sciences and Engineering Research Council of Canada.

References and Notes

(1) Hoff, A. J.; Deisenhofer, J. *Physics Reports* **1997**, *287*, 1.

(2) Martin, J. L.; Breton, J.; Hoff, A. J.; Migus, A.; Antonetti, A. *Proc. Natl. Acad. Sci. U.S.A.* **1986**, *83*, 957.

(3) Wraight, C. A.; Clayton, R. K. *Biochim. Biophys. Acta* **1974**, *333*, 246.

(4) Clayton, R. K. *Photochem. Photobiol.* **1962**, *1*, 201.

(5) Slooten, L. *Biochim. Biophys. Acta* **1972**, *256*, 452.

(6) Breton, J.; Martin, J.-L.; Migus, A.; Antonetti, A.; Orszag, A. *Proc. Natl. Acad. Sci. U.S.A.* **1986**, *83*, 5121.

(7) Breton, J.; Martin, J.-L.; Fleming, G. R.; Lambry, J.-C. *Biochemistry* **1988**, *27*, 8276.

(8) Jia, Y. W.; Jonas, D. M.; Joo, T. H.; Nagasawa, Y.; Lang, M. J.; Fleming, G. R. *J. Phys. Chem.* **1995**, *99*, 6263.

(9) Jonas, D. M.; Lang, M. J.; Nagasawa, Y.; Bradforth, S. E.; Dikshit, S. N.; Jimenez, R.; Joo, T.; Fleming, G. R. Ultrafast Energy Transfer within the Bacterial Photosynthetic RC. In *Proceedings of the Feldafing III Workshop*; Munich, 1995.

(10) Jonas, D. M.; Lang, M. J.; Nagasawa, Y.; Joo, T.; Fleming, G. R. *J. Phys. Chem.* **1996**, *100*, 12660.

(11) Stanley, R. J.; King, B.; Boxer, S. G. *J. Phys. Chem.* **1996**, *100*, 12052.
(12) Lin, S.; Taguchi, A. K. W.; Woodbury, N. W. *J. Phys. Chem.* **1996**, *100*, 17067.
(13) Haran, G.; Wynne, K.; Moser, C. C.; Dutton, P. L.; Hochstrasser, R. M. *J. Phys. Chem.* **1996**, *100*, 5562.
(14) Vos, M. H.; Breton, J.; Martin, J. L. *J. Phys. Chem. B* **1997**, *101*, 9820.
(15) King, B. A.; Stanley, R. J.; Boxer, S. G. *J. Phys. Chem. B* **1997**, *101*, 3644.
(16) Vulto, S. I. E.; Streltsov, A. M.; Shkuropatov, A. Y.; Shuvalov, V. A.; Aartsma, T. J. *J. Phys. Chem. B* **1997**, *101*, 7249.
(17) Arnett, D. C.; Moser, C. C.; Dutton, P. L.; Scherer, N. F. *J. Phys. Chem. B* **1999**, *103*, 2014.
(18) King, B. A.; McAnaney, T.; deWinter, A.; Boxer, S. G. *J. Phys. Chem. B* **2000**, *104*, 8895.
(19) Jackson, J. A.; Lin, S.; Taguchi, A. K. W.; Williams, J. C.; Allen, J. P.; Woodbury, N. W. *J. Phys. Chem. B* **1997**, *101*, 5747.
(20) Hutter, M. C.; Hughes, J. M.; Reimers, J. R.; Hush, N. S. *J. Phys. Chem. B* **1999**, *103*, 4906.
(21) Scholes, G. D.; Jordanides, X. J.; Fleming, G. R. *J. Phys. Chem. B* **2001**, *105*, 1640.
(22) Jordanides, X. J.; Scholes, G. D.; Fleming, G. R. *J. Phys. Chem. B* **2001**, *105*, 1652.
(23) Reed, D. W. *J. Biol. Chem.* **1969**, *244*, 4936.
(24) Philipson, K. D.; Sauer, K. *Biochemistry* **1973**, *12*, 535.
(25) Parson, W. W.; Cogdell, R. J. *Biochim. Biophys. Acta* **1975**, *416*, 105.
(26) Clayton, B. J.; Clayton, R. K. *Biochim. Biophys. Acta* **1978**, *501*, 470.
(27) Moss, D. A.; Leonhard, M.; Bauscher, M.; Maentele, W. *FEBS Lett.* **1991**, *283*, 33.
(28) Stocker, J. W.; Hug, S.; Boxer, S. G. *Biochim. Biophys. Acta* **1993**, *1144*, 325.
(29) Breton, J.; Nabedryk, E.; Parson, W. W. *Biochemistry* **1992**, *31*, 7503.
(30) Treynor, T. P.; Andrews, S. S.; Boxer, S. G. *J. Phys. Chem. B* **2003**, *107*, 11230.
(31) Walla, P. J.; Linden, P. A.; Hsu, C. P.; Scholes, G. D.; Fleming, G. R. *Proc. Natl. Acad. Sci. U.S.A.* **2000**, *97*, 10808.
(32) Scholes, G. D.; Fleming, G. R. *J. Phys. Chem. B* **2000**, *104*, 1854.
(33) Reimers, J. R.; Hush, N. S. *J. Am. Chem. Soc.* **1995**, *117*, 1302.
(34) Reimers, J. R.; Hush, N. S. *Chem. Phys.* **1995**, *197*, 323.
(35) Reimers, J. R.; Hutter, M. C.; Hush, N. S. *Photosynth. Res.* **1998**, *55*, 163.
(36) Reimers, J. R.; Hutter, M. C.; Hughes, J. M.; Hush, N. S. *Int. J. Quantum Chem.* **2000**, *80*, 1224.
(37) Parson, W. W.; Nabedryk, E.; Breton, J. *NATO ASI Ser., Ser. A* **1992**, *237*, 79.
(38) Scherer, P. O. J.; Fischer, S. F. Theoretical studies on the electron structure of the special pair dimer and the charge separation process for the reaction center *Rhodopseudomonas viridis*. In *NATO ASI Ser., Ser. A*, 1992; Vol. 237; p 193.
(39) Reimers, J. R.; Hush, N. S. *J. Chem. Phys.* **2003**, *119*, 3262.
(40) Reimers, J. R.; Shapley, W. A.; Hush, N. S. *J. Chem. Phys.* **2003**, *119*, 3240.
(41) Reimers, J. R.; Shapley, W. A.; Rendell, A. P.; Hush, N. S. *J. Chem. Phys.* **2003**, *119*, 3249.
(42) Krueger, B. P.; Scholes, G. D.; Fleming, G. R. *J. Phys. Chem. B* **1998**, *102*, 5378.
(43) Chappell, P. J.; Fischer, G.; Reimers, J. R.; Ross, I. G. *J. Mol. Spectrosc.* **1981**, *87*, 316.
(44) Becke, A. D. *J. Chem. Phys.* **1993**, *98*, 5648.
(45) Frisch, M. J.; Trucks, G. W.; Schlegel, H. B.; Scuseria, G. E.; Robb, M. A.; Cheeseman, J. R.; Zakrzewski, V. G.; Montgomery, J. A.; Stratmann, R. E.; Burant, J. C.; Dapprich, S.; Millam, J. M.; Daniels, A. D.; Kudin, K. N.; Strain, M. C.; Farkas, O.; Tomasi, J.; Barone, V.; Cossi, M.; Cammi, R.; Mennuci, B.; Pomelli, C.; Adamo, C.; Clifford, S.; Ochtersi, J.; Patterson, G. A.; Ayala, P. Y.; Cui, Q.; Morokuma, K.; Malick, D. K.; Rabuck, A. D.; Raghavachari, K.; Foresman, J. B.; Cioslowski, J.; Ortiz, J. V.; Stefanov, B. B.; Liu, G.; Liashenko, A.; Piskorz, P.; Komaromi, I.; Gomperts, R.; Martin, R. L.; Fox, D. J.; Keith, T.; Al-Laham, M. A.; Peng, C. Y.; Nanayakkara, A.; Gonzalez, G.; Challacombe, M.; Gill, P. M. W.; Johnson, B. G.; Chen, W.; Wong, M. W.; Andres, J. L.; Head-Gordon, M.; Replogle, E. S.; Pople, J. A. *Gaussian 98*, Revision A7; Gaussian Inc.: Pittsburgh, 1998.
(46) Cai, Z.-L.; Sendt, K.; Reimers, J. R. *J. Chem. Phys.* **2002**, *117*, 5543.
(47) Tozer, D. J.; Amos, R. D.; Handy, N. C.; Roos, B. O.; Serrano-Andr's, L. *Mol. Phys.* **1999**, *97*, 859.
(48) Hughes, J. M.; Hutter, M. C.; Reimers, J. R.; Hush, N. S. *J. Am. Chem. Soc.* **2001**, *123*, 8550.
(49) Ellis, R. L.; Kuehnlenz, G.; Jaffé, H. H. *Theor. Chim. Acta* **1972**, *26*, 131.
(50) McWeeny, R. *Methods of molecular quantum mechanics*, 2nd ed.; Academic Press: London, San Diego, 1989.
(51) Scholes, G. D.; Gould, I. R.; Cogdell, R. J.; Fleming, G. R. *J. Phys. Chem. B* **1999**, *103*, 2543.
(52) Jackson, J. D. *Classical electrodynamics*, 2d ed.; Wiley: New York, 1975.
(53) Buckingham, A. D. *Adv. Chem. Phys.* **1967**, *12*, 107.
(54) Buehler, R. J.; Hirschfelder, J. O. *Phys. Rev.* **1951**, *83*, 628.
(55) Buckingham, A. D. *Discuss. Faraday Soc.* **1965**, *No. 40*, 232.
(56) Stone, A. J. *The theory of intermolecular forces*; Clarendon Press: New York, 1996.
(57) Scholes, G. D.; Andrews, D. L. *J. Chem. Phys.* **1997**, *107*, 5374.
(58) Scherz, A.; Parson, W. W. *Biochim. Biophys. Acta* **1984**, *766*, 653.
(59) Breton, J. Low-temperature linear dicrosim study of the orientation of the pigments in reduced and oxidized reaction centers of *Rps.viridis* and *Rb. sphaeroides*. In *The photosynthetic bacterial reaction center: structure and dynamics*; Breton, J., Vermeglio, A., Eds.; Plenum Press: New York, 1988; Vol. I; p 59.
(60) Hartwich, G.; Scheer, H.; Aust, V.; Angerhofer, A. *Biochim. Biophys. Acta Bioenergetics* **1995**, *1230*, 97.
(61) Kirmaier, C.; Gaul, D.; Debey, R.; Holten, D.; Schenck, C. C. *Science* **1991**, *251*, 922.
(62) Steffen, M. A.; Lao, K. Q.; Boxer, S. G. *Science* **1994**, *264*, 810.
(63) Longuet-Higgins, H. C.; Rector, C. W.; Platt, J. R. *J. Chem. Phys.* **1950**, *18*, 1174.
(64) Rautter, J.; Lendzian, F.; Lubitz, W.; Wang, S.; Allen, J. P. *Biochemistry* **1994**, *33*, 12077.
(65) Lendzian, F.; Huber, M.; Isaacson, R. A.; Endeward, B.; Plato, M.; Boenigk, B.; Moebius, K.; Lubitz, W.; Feher, G. *Biochim. Biophys. Acta* **1993**, *1183*, 139.
(66) Zhou, H.; Boxer, S. G. *J. Phys. Chem. B* **1998**, *102*, 9139.
(67) Moore, L. J.; Zhou, H.; Boxer, S. G. *Biochemistry* **1999**, *38*, 11949.
(68) Reimers, J. R.; Hush, N. S. *Inorg. Chim. Acta* **1994**, *226*, 33.
(69) Jordanides, X. J., unpublished results.
(70) Treynor, T. P., personal communication.
(71) Sauer, K.; Dratz, E. A.; Coyne, L. *Proc. Natl. Acad. Sci. U.S.A.* **1968**, *61*, 17.
(72) Breton, J.; Nabedryk, E.; Clerici, A. *Vib. Spectrosc.* **1999**, *19*, 71.
(73) Breton, J. *Biochim. Biophys. Acta Bioenergetics* **1985**, *810*, 235.
(74) Shreve, A. P.; Cherepy, N. J.; Franzen, S.; Boxer, S. G.; Mathies, R. A. *Proc. Natl. Acad. Sci. U.S.A.* **1991**, *88*, 11207.
(75) Cherepy, N. J. Electronic and Nuclear Dynamics of the Bacterial Photosynthetic Reaction Center and Chorosomes from Resonance Raman Intensities; Ph.D. Thesis, University of California, Berkeley, 1996.
(76) Groot, M. L.; Yu, J. Y.; Agarwal, R.; Norris, J. R.; Fleming, G. R. *J. Phys. Chem. B* **1998**, *102*, 5923.
(77) Harcourt, R. D.; Ghiggino, K. P.; Scholes, G. D.; Steer, R. P. *J. Chem. Phys.* **1998**, *109*, 1310.
(78) Pyernik, M.; Perets, E.; Scharf, B. E. *J. Mol. Spectrosc.* **1995**, *169*, 315.
(79) Scholes, G. D. *Annu. Rev. Phys. Chem.* **2003**, *54*, 57−87.